LANGMUIR

Open Access
This article is licensed under CC-BY 4.0

pubs.acs.org/Langmuir
Article

Incorporation of Oligo(Styrene), Oligo(Butadiene), Oligo(Methyl Methacrylate), and Oligo(*tert*-Butyl Acrylate) Droplets in Giant Unilamellar Vesicles

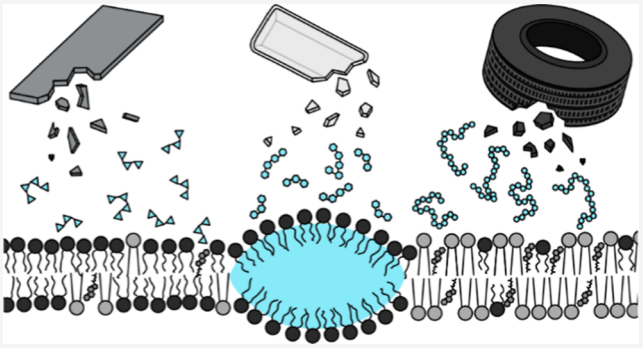
Chiho Kataoka-Hamai,* Waka Nakanishi, and Shinya Hattori

Cite This: *Langmuir* 2026, 42, 24915−24925

Read Online

ACCESS | Metrics & More | Article Recommendations | Supporting Information

ABSTRACT: In the environment, microplastics fragment and degrade into plastic oligomers, posing potential risks to ecosystems and human health. In the present study, the interactions between giant unilamellar vesicles (GUVs) and liquid droplets of oligo(styrene), oligo(butadiene), oligo(methyl methacrylate), and oligo(*tert*-butyl acrylate) were investigated using fluorescence microscopy. GUVs were used in a homogeneous fluid state or in a phase-separated state consisting of either a liquid-disordered (L_d) phase and a solid-ordered (S_o) phase, or a L_d phase and a liquid-ordered (L_o) phase. The effects of plastic oligomers on membrane structures vary depending on the oligomer type. Oligo(styrene), oligo(butadiene), and oligo(*tert*-butyl acrylate) droplets were homogeneously embedded between the monolayer leaflets, whereas the oligo(methyl methacrylate) droplets were bound to the bilayers through inhomogeneous membrane structures, regardless of the lipid composition. The bilayer phase separations were retained after oligomer incorporation, except for the L_d/S_o phase-separated bilayer exposed to oligo(*tert*-butyl acrylate). In this exceptional case, no domain structures were visible in the fluorescence images. In the L_d/S_o phase-separated bilayer, the oligo(styrene) and oligo(butadiene) droplets were distributed exclusively in the L_d phase, and were all pinned at the domain boundaries. In the L_d/L_o phase-separated bilayer, the oligo(styrene), oligo(butadiene), and oligo(*tert*-butyl acrylate) droplets invariably localized to the L_d phase, with approximately half anchored to domain boundaries. The data also suggested that in the L_d/S_o bilayer, oligo(methyl methacrylate) molecules were predominantly partitioned into the L_d phase, whereas in the L_d/L_o bilayer, they were slightly more soluble in the L_d phase than in the L_o phase. Furthermore, the slight solubility of oligo(methyl methacrylate) in water enabled its incorporation into homogeneous fluid bilayers via two pathways: transfer from an in-bilayer droplet to the matrix bilayer and transfer from aqueous solution.

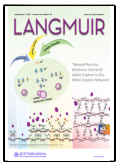


INTRODUCTION

Since the mass production of plastics began less than a century ago,[1,2] plastic pollution has become a critical problem. From 1950 to 2015, approximately 60% of total plastic production has entered landfills or been emitted into the natural environment.[1] These plastics accumulate in the environment because of their high persistence.[3] These accumulated plastics then fragment and degrade into smaller pieces via mechanical stress, photo-oxidation, and enzymatic reactions.[3,4] According to the definition proposed by Hartmann et al.,[5] plastic fragments in the size ranges of 1−1000 μm and 1−1000 nm are referred to as microplastics (MPs) and nanoplastics (NPs), respectively. MPs and NPs serve as vectors of toxic hydrophobic materials including plastic additives and organic contaminants.[6,7] Currently, these fragments are ubiquitous across the planet and have been detected in various biological species including humans.[3,4] Therefore, the risks they pose to ecosystems and human health are of considerable concern.[3] Further fragmentation of MPs and NPs generates plastic oligomers,[4] and recent studies suggest that these oligomers are potential pollutants.[8−11] Thus, understanding the influence of MPs, NPs, and plastic oligomers on biological cells is of considerable importance.

At the onset of an interaction with a cell, a plastic particle or oligomer molecule encounters the cell membrane. Therefore, it is important to study the interactions between plastic particles or oligomers and phospholipid bilayers. Previous studies have used molecular dynamics simulations to investigate the interactions between bilayers and NPs formed of oligo(styrene),[12−15] oligo(ethylene),[12,16,17] oligo(propylene),[12,18] or oligo(ethylene terephthalate),[19] comprising a few to ∼100

Received: May 8, 2026
Revised: July 17, 2026
Accepted: July 17, 2026
Published: July 31, 2026



ACS Publications
© 2026 The Authors. Published by American Chemical Society

https://doi.org/10.1021/acs.langmuir.6c02733
Langmuir 2026, 42, 24915−24925

Downloaded from pubs.acs.org/langd5/article-pdf/42/34/24915/6635134/acs.langmuir.6c02733.pdf by NATL INST FOR MATLS SCIENCE (NIMS), Chiho Kataoka-Hamai on 02 September 2026

repeat units. These simulation studies suggested spontaneous oligomer incorporation in the hydrophobic regions of the lipid bilayer. In addition, several experimental studies were performed. A study using free-standing bilayers showed that bilayer tension increased after adsorption of poly(ethylene), poly(styrene) (PS), or poly(methyl methacrylate) (PMMA) microparticles with diameters of ∼1−10 μm.[20] A recent study on the interaction between PS NPs and giant unilamellar vesicles (GUVs) reported that NPs induced membrane permeabilization depending on the shape of the NPs.[21] Another experimental study investigated the effect of oligo(styrene) on the phase behavior of pure 1,2-dipalmitoyl-*sn*-glycero-3-phosphocholine (DPPC) and binary mixtures of DPPC and 1,2-dioleoyl-*sn*-glycero-3-phosphocholine (DOPC).[22] This previous study indicated that the melting temperature of the DPPC bilayer and the miscibility transition temperature of the DOPC/DPPC bilayers decreased after oligomer incorporation. Despite the increasing interest in the influence of plastics on bilayers, further experimental studies are required to elucidate plastic−bilayer interactions.

In the present study, the interactions of GUVs with oligo(styrene), oligo(butadiene), oligo(methyl methacrylate), and oligo(*tert*-butyl acrylate) were investigated (Figure 1).

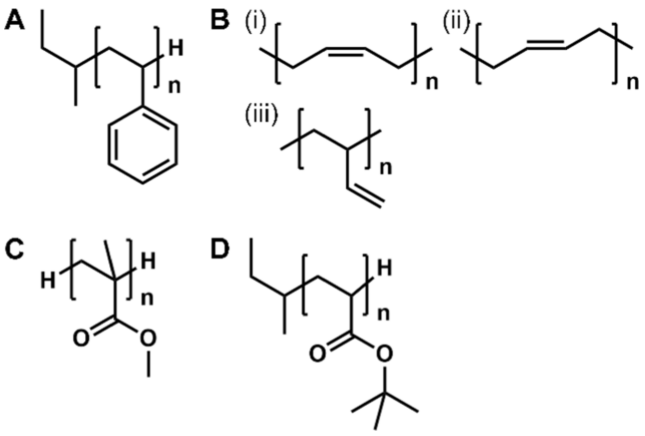


Figure 1. Chemical structures of the plastic oligomers used in the present study. (A) *Sec*-butyl-terminated oligo(styrene) (n = 4). (B) Oligo(butadiene) (a mixture of 1,4-*cis* (i), 1,4-*trans* (ii), and *vinyl* (iii) isomers, with a number-average molar mass of ∼5000 g/mol). (C) Oligo(methyl methacrylate) (n = 3). (D) *Sec*-butyl-terminated oligo(*tert*-butyl acrylate) (n = 3).

Oligo(styrene) (Figure 1A) comprises four styrene units. PS is used for diverse applications such as packaging, and is a major contributor to global plastic waste.[1,23] PS MPs have been detected in human blood and tissues.[24,25] In addition, oligo(styrene) has been detected in seawater and sand samples.[26] A recent study predicted that oligo(styrene) is more toxic than styrene monomer to aquatic and terrestrial organisms, even though the monomer is classified as a Group 2A agent (probably carcinogenic to humans) by the International Agency for Research on Cancer.[27] Oligo(butadiene) (Figure 1B) is a low-molecular-weight poly(butadiene) comprising ∼90 butadiene units on average. High-molecular-weight poly(butadiene) is a synthetic rubber widely used in automobile tires and is a major constituent of the MPs generated by terrestrial vehicles, denoted as tire wear particles.[5,28] Oligo(methyl methacrylate) (Figure 1C) is a trimer. PMMA is generally used as an alternative to inorganic glass. Despite its low fraction of total global plastic production,[23] PMMA is a major component of the MPs collected from seawater samples, potentially because it is widely used for ship coatings.[29] In addition, PMMA MPs have been found in human blood and tissues, presumably because this polymer is widely used for daily products and medical devices, such as cosmetics and dental materials.[24,25] Finally, oligo(*tert*-butyl acrylate) (Figure 1D) comprises three monomeric units. Poly(*tert*-butyl acrylate) (P*t*BA) is not commonly used as a plastic material; thus, this oligomer was investigated to allow for comparison with oligo(methyl methacrylate).

It is generally challenging to incorporate oil molecules in bilayers.[14] However, a previous study on intracellular lipid droplets reported a simple method for incorporating droplets of biological liquid oils, including triacylglycerols and cholesteryl esters, into GUVs.[30−32] In this method, vesicles are incubated with an oil-in-water emulsion to spontaneously incorporate oil droplets between the monolayer leaflets of bilayers.[30−32] This method was used to study the behavior of plastic oligomer droplets and molecules in model bilayer membranes.

In this study, the interactions of oligo(styrene), oligo(butadiene), oligo(methyl methacrylate), and oligo(*tert*-butyl acrylate) with GUVs in a homogeneous fluid state or a phase-separated state were investigated using fluorescence microscopy. Two phase-separated bilayers consisting of either a liquid-disordered (L_d) phase and a solid-ordered (S_o) phase, or a L_d phase and a liquid-ordered (L_o) phase were studied. Herein, various behaviors of plastic oligomers and their droplets, which depend on oligomer type, are demonstrated. Those behaviors comprise homogeneous or inhomogeneous droplet incorporation into bilayers, preferential partitioning of droplets and oligomer molecules into the more fluid phase of phase-separated systems, droplet pinning to domain boundaries, the disappearance of domain structures, and oligomer partitioning into bilayers from aqueous solution.

EXPERIMENTAL SECTION

Materials

DOPC, DPPC, and 1,2-dioleoyl-*sn*-glycero-3-phosphoethanolamine (DOPE) were purchased from Avanti Polar Lipids (Alabaster, AL, USA). The concentrations of the phospholipid stock solutions in chloroform were determined by phosphorus assay.[33] Cholesterol was purchased from Nu-Check Prep (Elysian, MN, USA). The concentration of the cholesterol stock solution in chloroform was determined using a colorimetric assay kit (FUJIFILM Wako Pure Chemical Corporation, Osaka, Japan). Texas Red (TR) 1,2-dihexadecanoyl-*sn*-glycero-3-phosphoethanolamine, triethylammonium salt (TR-DHPE) was purchased from Thermo Fisher Scientific (Waltham, MA, USA). Fluorescent probe 1,2-dipalmitoyl-*sn*-glycero-3-phosphoethanolamine-*N*-(7-nitro-2−1,3-benzoxadiazol-4-yl) (ammonium salt) (NBD-DPPE) was purchased from Avanti Polar Lipids (Alabaster, AL, USA). Lipi-Blue was purchased from Dojindo Laboratories (Kumamoto, Japan).[34]

All plastic oligomers used in this study are liquid at room temperature. *Sec*-butyl-terminated oligo(styrene) (Figure 1A) was purchased from Tosoh Corporation (Tokyo, Japan; catalog no. TSKgel standard PS A-300). This oligomer has a mass-average molar mass (M_w)/number-average molar mass (M_n) ratio of 1.17 and an M_n value of 387 g/mol. Oligo(butadiene) (Figure 1B) with an M_n value of ∼5000 g/mol was purchased from Sigma-Aldrich (St. Louis, MO, USA). It consisted of the *cis* and *trans* isomers (80%) and the *vinyl* isomer (20%). Oligo(methyl methacrylate) with an M_w/M_n value of 1.00 and an M_n value of 302 g/mol (Figure 1C) was purchased from

Downloaded from pubs.acs.org/langd5/article-pdf/42/34/24915/6635134/0/acs.langmuir.6c02733.pdf by NATL INST FOR MATLS SCIENCE (NIMS), Chiho Kataoka-Hamai on 02 September 2026

https://doi.org/10.1021/acs.langmuir.6c02733
Langmuir 2026, 42, 24915−24925

Agilent Technologies (Santa Clara, CA, USA; catalog no. PSS-MM302). The chemical structure of the monomeric unit of this oligomer was disclosed. However, the overall chemical structure is unknown. Therefore, the molecular structure was characterized using proton nuclear magnetic resonance (^{1}H NMR) spectroscopy. The NMR spectrum of a sample in deuterated chloroform ($CDCl_3$) was recorded on a JNM-ECZL600R spectrometer operated at 600 MHz (JEOL, Tokyo, Japan). The NMR data (Figures S1−S4) confirmed that the reagent comprised a diastereomeric mixture of the PMMA oligomers in which three repeat units were linked in the regular head-to-tail orientation. *Sec*-butyl-terminated oligo(*tert*-butyl acrylate) (Figure 1D) with an M_w/M_n value of 1.04 and an M_n value of 430 g/mol was purchased from Polymer Source (Quebec, Canada; catalog no. P9348C-tBuA).

Surface Pressure Measurements at the Air/Water Interface

Surface pressure measurements at the air/water interface were performed for oligo(methyl methacrylate) and oligo(*tert*-butyl acrylate) using a Langmuir trough (35 cm × 7.5 cm) equipped with two barriers (KSV NIMA, Biolin Scientific, Gothenburg, Sweden). Each oligomer in chloroform (0.5 or 1 mM) was spread on pure water (23 °C). The subphase temperature was controlled using a water circulator. The solvent was allowed to evaporate for 10 min before compression. The surface pressure was recorded with a platinum Wilhelmy plate (perimeter, 20 mm) at a compression rate of 15 mm/min.

Preparation of GUVs

The GUVs were prepared by electroformation using the following procedure.[35,36] The lipids were mixed with the desired composition in chloroform to yield a total lipid concentration of 3.5 mM. The lipid compositions are expressed as molar ratios within the nonfluorescent lipids. TR-DHPE (0.2 mol %) was added to DOPC, DOPC/DOPE (9:1), and DOPC/DPPC (1:1), whereas TR-DHPE (0.1 mol %) and NBD-DPPE (0.2 mol %) were added to DOPC/DPPC/cholesterol (3:3:2). The lipid solutions in chloroform were spread onto two platinum electrodes (0.5 mm diameter) separated by ∼1 mm. After solvent evaporation under a nitrogen gas stream, the electrodes were immersed in 300 mM sucrose to yield a lipid concentration of 0.22 mM. Subsequently, a sinusoidal alternating voltage with a peak-to-peak amplitude of 2.2 V was applied for 35 min using a function generator (PCGU-1000, Velleman, Gavere, Belgium). The frequencies during the first 30 min and the final 5 min were 10 and 2 Hz, respectively. During the voltage application, the DOPC and DOPC/DOPE (9:1) samples were held at room temperature. However, the voltage was applied to the DOPC/DPPC (1:1) and DOPC/DPPC/cholesterol (3:3:2) samples at 55 °C, exceeding the melting temperature of DPPC (41.4 °C) and the miscibility transition temperature of DOPC/DPPC/cholesterol (3:3:2) (∼33 °C).[37,38]

Incorporation of Plastic Oligomer Droplets in GUVs

Oil droplets were incorporated into GUVs similarly to a previously reported method for triacylglycerol and cholesteryl ester droplets.[30−32] Lipi-Blue was added to the oligomers at a concentration of 0.003 mol % relative to the monomer residue. Lipi-Blue was previously developed to stain intracellular lipid droplets.[34] The dye does not stain lipid bilayers, but has a strong affinity for hydrophobic molecules. Its fluorescence is greatly enhanced in hydrophobic environments.[34] The Lipi-Blue-labeled oil samples (0.5 μL) were mixed with an aqueous solution (4.5 μL) containing 40 mM NaCl, 191 mM sucrose, and 10 mM sodium phosphate (pH 7.4). NaCl was added to enhance droplet incorporation efficiency.[31] Sucrose was added to avoid significantly changing the osmotic pressure across the bilayers after the subsequent mixing of this oil/water mixture with a GUV solution. The oil/water mixture was sonicated for 30 min in an ultrasonic bath, vortexed, and further sonicated for an additional 30 min. Immediately after the second sonication, the oil suspension (5 μL) was mixed with a GUV sample (0.22 mM lipid, 5 μL) by pipetting slowly four times, followed by incubation for 30 min. Incubation with the DOPC and DOPC/DOPE (9:1) samples was performed on a rotating mixer at room temperature. In contrast, incubation with the DOPC/DPPC (1:1) and DOPC/DPPC/cholesterol (3:3:2) samples was performed in a block heater held at 55 °C, while tapping every 5 min. After incubation of the DOPC/DPPC/cholesterol (3:3:2) mixtures with the oil suspensions, the samples were cooled from 55 to 25 °C at a rate of 0.1 °C/s using a thermal cycler (MyCycler, Bio-Rad, Hercules, CA, USA). After incubation of all the other vesicle samples with the oil suspensions, the samples were transferred to a bench at ambient temperature.

Confocal Laser Scanning Microscopy

Round glass coverslips (25 mm diameter, no.1, Matsunami Glass Ind., Ltd., Osaka, Japan) were rinsed with ethanol and dried in a nitrogen stream. The cleaned coverslips were stored in air until use. The oil/vesicle mixtures (10 μL) were diluted in 300 mM glucose (146 μL), then deposited onto a glass coverslip in a poly(dimethylsiloxane) chamber attached to the coverslip surface under light pressure. The glucose solution was used to sediment vesicles near the glass surface. The coverslips were fixed in Attofluor cell chambers (Thermo Fisher Scientific, Waltham, MA, USA).

Confocal imaging was performed with a Zeiss LSM 900 microscope (Carl Zeiss, Oberkochen, Germany) at 63× magnification using a 1.40-numerical aperture (NA) oil-immersion objective. TR-DHPE, NBD-DPPE, and Lipi-Blue were excited at 561, 488, and 405 nm, respectively. For samples dual-labeled with TR-DHPE and Lipi-Blue, excitation and detection were performed simultaneously. In contrast, sequential excitation and detection were used for samples labeled with TR-DHPE/NBD-DPPE and TR-DHPE/NBD-DPPE/Lipi-Blue to minimize bleed-through. Two GaAsP detectors were used to detect the two fluorophores, whereas the GaAsP detectors and an Airyscan 2 imaging device were used to detect the three fluorophores. The bilayer structures before plastic oligomer incorporation were confirmed by confocal fluorescence imaging (Figure S5).

Epi-Fluorescence Microscopy for Supported Lipid Bilayer (SLB) Patches

SLB patches were formed on glass as follows. Square glass coverslips (22 × 22 mm, no. 1, Matsunami Glass Ind., Ltd., Osaka, Japan) were sonicated in acetone for 3 min three times and then in ethanol for 3 min three times in an ultrasonic bath. The cleaned coverslips were stored in ethanol. Immediately before use, the coverslips were dried under a nitrogen gas stream, followed by a 2 min exposure to air plasma generated with a PDC-32G plasma cleaner (Harrick Plasma, Ithaca, NY, USA). The oil/vesicle mixtures (10 μL) were diluted in a solution containing NaCl and glucose to yield 0.0067 mM lipid, 42 mM NaCl, and 270 mM glucose. They were subsequently deposited onto the cleaned coverslip surface in a poly(dimethylsiloxane) chamber. After adsorption for 15 min, the glass surface was rinsed with a solution containing 40 mM NaCl and 10 mM sodium phosphate (pH 7.4) to remove unbound vesicles and oil droplets.

The SLB patches were examined with an Eclipse Ti-E microscope (Nikon, Tokyo, Japan) equipped with an electron-multiplying charge-coupled device camera (iXon EM + 897E, Andor Technology, Belfast, UK). The samples were imaged using 10× (NA 0.45) and 40× (NA 0.95) objectives under light-emitting diode illumination (X-Cite Xylis XT720L, Excelitas Technologies Corp., Pittsburgh, PA, USA). The filter sets used for TR-DHPE and Lipi-Blue were FF01-561/12:Di01-R561:FF01 609/54 and FF01-378/52-25: FF409-Di03-25 × 36: FF02-447/60-25, respectively (Semrock, IDEX Health & Science, Oak Harbor, WA, USA). The net Lipi-Blue fluorescence intensities from SLB patches were determined by subtracting the fluorescence signals from the glass surface using ImageJ.[39]

Experimental Values

The reported values are the mean (±standard error) of N determinations.

Downloaded from pubs.acs.org/langd5/article-pdf/42/34/24915/6351340/acs.langmuir.6c02733.pdf by NATL INST FOR MATLS SCIENCE (NIMS), Chiho Kataoka-Hamai on 02 September 2026

https://doi.org/10.1021/acs.langmuir.6c02733
Langmuir 2026, 42, 24915−24925

RESULTS AND DISCUSSION

Surface Pressure Measurements of Oligo(methyl Methacrylate) and Oligo(*tert*-butyl Acrylate) at the Air/Water Interface

Oligo(styrene) and oligo(butadiene) (Figure 1A,B) are hydrocarbons and therefore have no amphiphilic properties. However, oligo(methyl methacrylate) and oligo(*tert*-butyl acrylate) (Figure 1C,D) may be amphiphilic as a result of the ester bonds in the structures. Notably, previous studies have reported that PMMA and P*t*BA form monolayers at the air/water interface.[40−42] Therefore, to understand their surface activities, surface pressure measurements were performed at the air/water interface. The data for oligo(*tert*-butyl acrylate) (Figure 2, red) showed that the surface pressure increased as

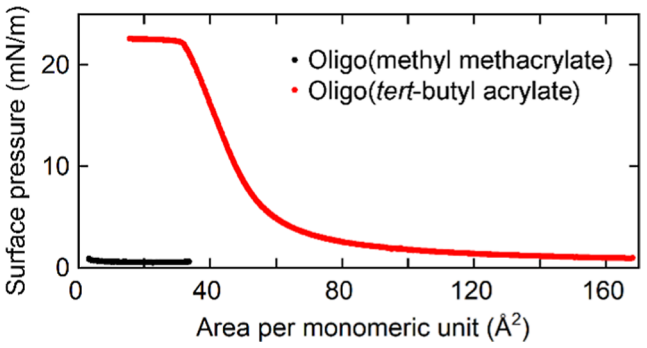


Figure 2. Surface pressure data for oligo(methyl methacrylate) (black) and oligo(*tert*-butyl acrylate) (red) at the air/water interface.

the interfacial area decreased and eventually reached a plateau at 22.1 (±0.03) mN/m (N = 3). This result is consistent with that previously reported for P*t*BA monolayers.[42] Thus, oligo(*tert*-butyl acrylate) appears to form the interfacial monolayer. In contrast, the compression of oligo(methyl methacrylate) (Figure 2, black) resulted in no significant surface pressure even when a large amount of the oligomer was spread on the interface. These data indicate that oligo(methyl methacrylate) was slightly soluble in water, dissolving in subphase water upon spreading at the interface and during the subsequent compression. The high aqueous solubility of oligo(methyl methacrylate) compared with that of oligo(*tert*-butyl acrylate) is reasonable. There are two reasons for this: first, the methyl methacrylate monomer is ∼10 times more soluble in water (solubility, ∼0.15 mol/L) than the *tert*-butyl acrylate monomer (∼0.016 mol/L); second, the oligo(*tert*-butyl acrylate) is *sec*-butyl-terminated, whereas oligo(methyl methacrylate) is not (Figure 1).

Incorporation of Oligo(styrene), Oligo(butadiene), and Oligo(*tert*-butyl Acrylate) Droplets in DOPC and DOPC/DOPE (9:1) GUVs

Oligo(styrene), oligo(butadiene), and oligo(*tert*-butyl acrylate) droplets were incorporated in homogeneous fluid bilayers, DOPC (Figure 3), and DOPC/DOPE (9:1) (Figure S6). For each oligomer−lipid composition pair, 5−13 vesicles (diameter: ∼3−24 μm) were observed. The vesicles and oligomers were labeled with TR-DHPE and Lipi-Blue, respectively.[34] The confocal fluorescence data of these vesicles revealed the following features. First, the TR fluorescence signals on or near the droplet surfaces were homogeneous (Figures 3A−C and S6, panel ii). This result indicates that the oligomer droplets were incorporated between the monolayer leaflets. Second, the droplets diffused laterally within the bilayer over time (Figure 3D). Finally, the Lipi-Blue fluorescence intensities in the bilayers were quite low (Figure 3A−C and S6, panel iii). Because Lipi-Blue does not stain pure lipid bilayers,[34] the low Lipi-Blue fluorescence emission indicates no significant change in bilayer composition.

Incorporation of Oligo(styrene), Oligo(butadiene), and Oligo(*tert*-butyl Acrylate) Droplets in DOPC/DPPC (1:1) GUVs

A DOPC/DPPC (1:1) mixture containing TR-DHPE was used as a model bilayer with L_d/S_o phase separation.[43] In this bilayer system, TR-DHPE is partitioned into the L_d phase. A total of 12 vesicles (diameter: ∼7−15 μm) containing 1−3 oligo(styrene) droplets each (the total number of the analyzed droplets: 17), 11 vesicles (diameter: ∼5−11 μm) containing one or two oligo(butadiene) droplets each (the total number of the droplets: 15), and 18 vesicles (diameter: ∼5−13 μm) containing 1−3 oligo(*tert*-butyl acrylate) droplets each (the total number of the droplets: 17) were analyzed. TR fluorescence intensities on or near the droplet surfaces were homogeneous after incorporating oligo(styrene) (Figure 4A), oligo(butadiene) (Figure 4B), and oligo(*tert*-butyl acrylate) droplets (Figure 4C). Therefore, the droplets were likely surrounded homogeneously by the monolayer leaflets.

L_d/S_o phase separation was maintained in the presence of oligo(styrene) (Figure 4A) and oligo(butadiene) droplets (Figure 4B). These oligomer droplets were exclusively incorporated into the L_d phase. Additionally, the droplets were always anchored to the domain boundaries, as shown in Figure 4A panels ii (arrows), iv, and v and Figure 4B. Both the L_d and S_o phases exhibited negligible Lipi-Blue fluorescence.

In contrast to oligo(styrene) and oligo(butadiene), which had no significant effect on the domain structures, oligo(*tert*-butyl acrylate) had a strong influence (Figure 4C and S7). No domain structures were visible in any of the DOPC/DPPC (1:1) vesicles incorporating oligo(*tert*-butyl acrylate) droplets.

Incorporation of Oligo(styrene), Oligo(butadiene), and Oligo(*tert*-butyl Acrylate) Droplets in DOPC/DPPC/Cholesterol (3:3:2) GUVs

A DOPC/DPPC/cholesterol (3:3:2) mixture containing TR-DHPE and NBD-DPPE was used as a model bilayer with L_d/L_o phase separation.[32,35] TR-DHPE and NBD-DPPE are predominantly partitioned into the L_d and L_o phases, respectively.[32] In vesicles with this lipid composition, oligo(styrene), oligo(butadiene) and oligo(*tert*-butyl acrylate) droplets were incorporated. A total of 29 vesicles (diameter: ∼8−21 μm) containing 1−8 oligo(styrene) droplets each (the total number of the analyzed droplets: 57), 24 vesicles (diameter: ∼7−19 μm) containing 1−4 oligo(butadiene) droplets each (the total number of the droplets: 52), and 22 vesicles (diameter: ∼4−10 μm) containing one oligo(*tert*-butyl acrylate) droplet each (the total number of the droplets: 22) were analyzed. The incorporation of these oligomers did not affect the fluorescence patterns of the domain structures (Figure 5). These droplets were exclusively partitioned in the L_d phase. Among these, 46% of the oligo(styrene) droplets, 44% of the oligo(butadiene) droplets, and 50% of the oligo(*tert*-butyl acrylate) droplets were anchored to the domain boundaries (Figure 5A). The remaining droplets did not contact any visible domain boundaries in the fluorescence images (Figure 5B).

Downloaded from pubs.acs.org/langd5/article-pdf/42/34/24915/6351340/acs.langmuir.6c02733.pdf by NATL INST FOR MATLS SCIENCE (NIMS), Chiho Kataoka-Hamai on 02 September 2026

https://doi.org/10.1021/acs.langmuir.6c02733
Langmuir 2026, 42, 24915−24925

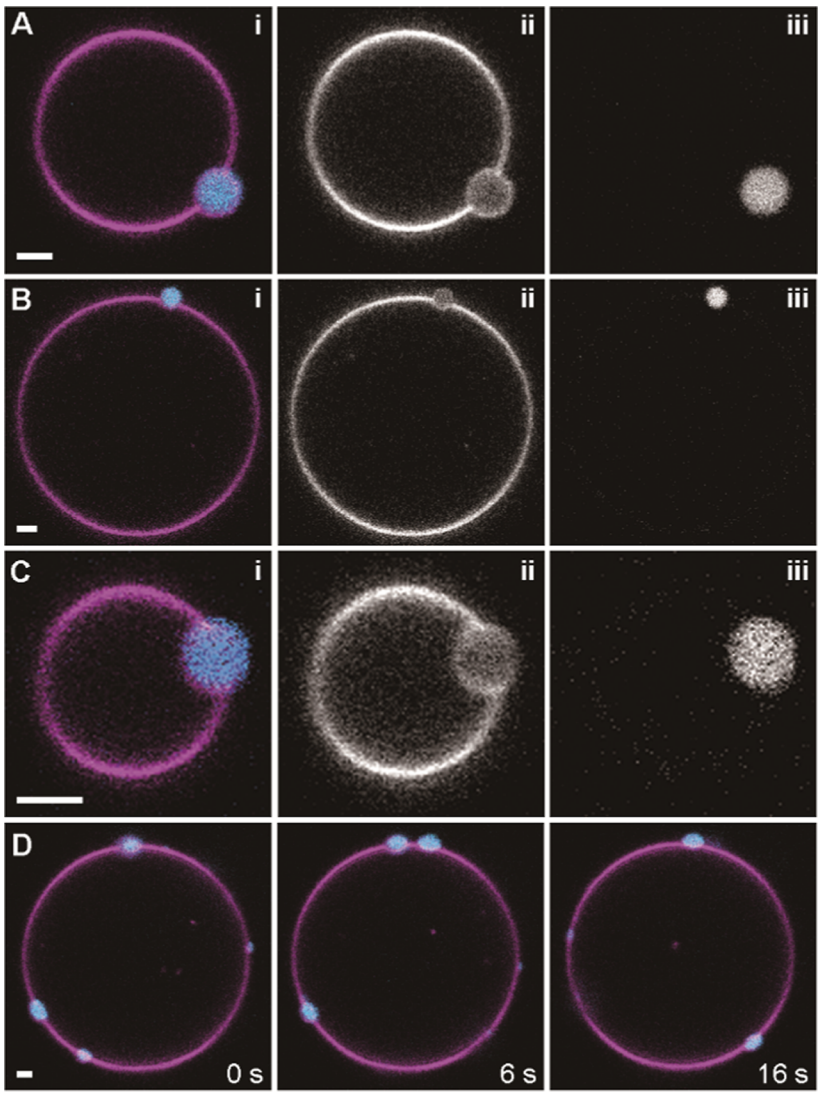


Figure 3. Confocal fluorescence images obtained for DOPC GUVs incorporating (A,D) oligo(styrene), (B) oligo(butadiene), and (C) oligo(*tert*-butyl acrylate) droplets. The color data present the overlay images of TR (magenta) and Lipi-Blue (light blue) fluorescence signals. (A−C) The grayscale images are the TR (panel ii) and Lipi-Blue (panel iii) channel images. (D) Images of the droplet migration recorded at 0 s (left), 6 s (middle), and 16 s (right). The scale bars are 2 μm.

Incorporation of Oligo(methyl Methacrylate) Droplets in GUVs

For all studied lipid compositions, i.e., DOPC (10 vesicles with diameters of ∼5−13 μm), DOPC/DOPE (9:1) (11 vesicles with diameters of ∼5−17 μm), DOPC/DPPC (1:1) (9 vesicles with diameters of ∼4−10 μm), and DOPC/DPPC/cholesterol (3:3:2) (9 vesicles with diameters of ∼4−13 μm), oligo(methyl methacrylate) droplets were bound to the bilayers via complex membrane structures (Figure 6). It was therefore unlikely that the droplets were surrounded homogeneously by the monolayer leaflets. The surface pressure data (Figure 2) suggested that oligo(methyl methacrylate) had higher water solubility (i.e., greater hydrophilicity) than the other oligomers. Therefore, it was expected that the oligomer interacted with both hydrophobic tails and hydrophilic headgroups in the phospholipids. These interactions likely led to inhomogeneous droplet incorporation.

The DOPC and DOPC/DOPE (9:1) bilayers associated with oligo(methyl methacrylate) droplets produced considerable Lipi-Blue fluorescence signals (Figure 6A). This result indicates that the bilayer composition changed significantly after droplet incorporation, suggesting that oligomers likely diffused into the bilayer. In addition, the droplet-free bilayers produced non-negligible Lipi-Blue fluorescence emission (Figure 6B), suggesting that the bilayers adsorbed oligomer molecules dissolved in the aqueous phase. Nevertheless, the droplet-incorporating bilayers tended to generate higher Lipi-Blue fluorescence intensities than those with no droplets (Figure 6B). However, the fluorescence intensities in the confocal images were not analyzed because of photobleaching. Instead, as described in the next section, the Lipi-Blue fluorescence intensities from SLB patches were examined using epi-fluorescence microscopy.

When oligo(methyl methacrylate) droplets were incorporated into the DOPC/DPPC (1:1) vesicles (Figure 6C), the L_d domains showed Lipi-Blue fluorescence signals, but the S_o domains did not (panels iii and vi). Therefore, the oligomer likely penetrated the L_d phase, but not the S_o phase.

In the DOPC/DPPC/cholesterol (3:3:2) vesicles with oligo(methyl methacrylate) droplets, both L_d and L_o phases

https://doi.org/10.1021/acs.langmuir.6c02733
Langmuir 2026, 42, 24915−24925

Downloaded from pubs.acs.org/langd5/article-pdf/42/34/24915/6351340/acs.langmuir.6c02733.pdf by NATL INST FOR MATLS SCIENCE (NIMS), Chiho Kataoka-Hamai on 02 September 2026

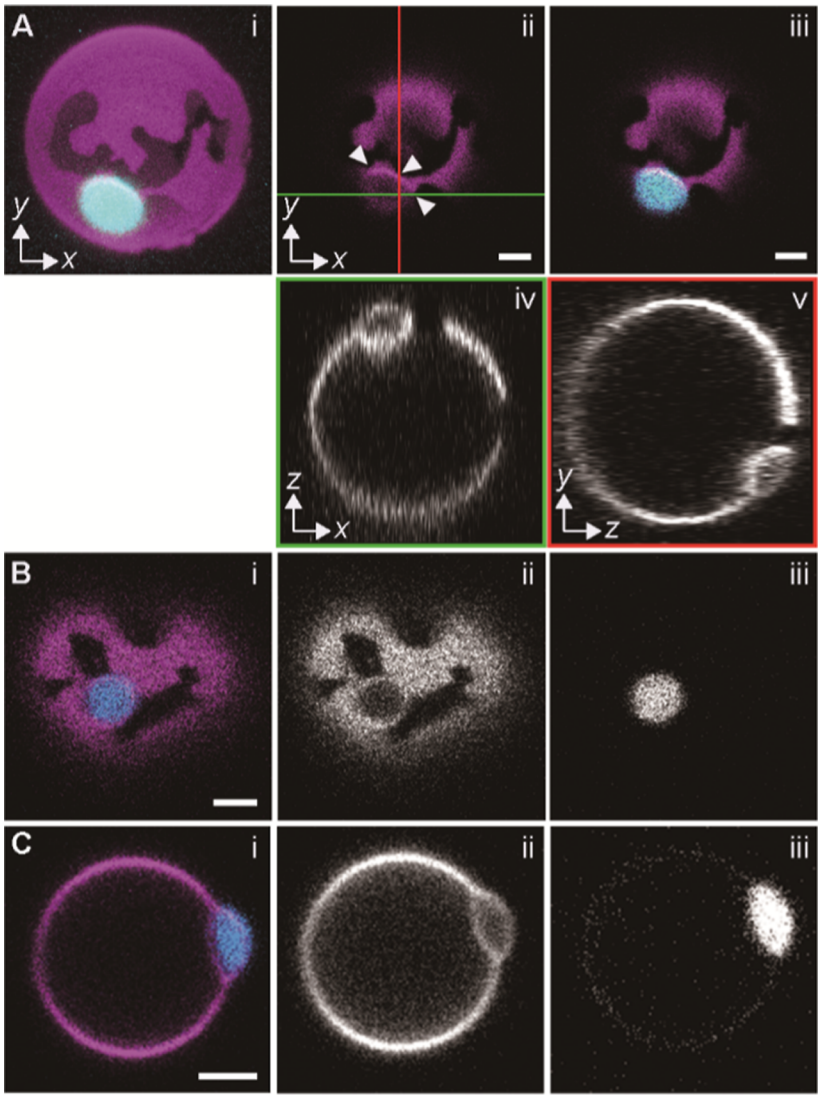


Figure 4. Confocal fluorescence images of DOPC/DPPC (1:1) GUVs with (A) an oligo(styrene) droplet, (B) an oligo(butadiene) droplet, and (C) an oligo(*tert*-butyl acrylate) droplet. The color images show fluorescence signals from TR-DHPE (magenta) and Lipi-Blue (light blue). (A) Fluorescence images of a GUV (diameter: 13.7 μm). (i) The three-dimensional image viewed from the coverslip surface ($x-y$ plane) was constructed from 38 slices. (ii, iii) The fifth-slice images of TR (panel ii) and both dyes (panel iii). (ii) The arrows indicate the positions at which the droplet rim was anchored to the domain boundaries. (iv) The cross-sectional TR fluorescence image obtained along the green line in panel ii. (v) The cross-sectional TR fluorescence image obtained along the red line in panel ii. (B, C) Two-dimensional fluorescence images of both dyes (panel i), TR (panel ii), and Lipi-Blue (panel iii). (C) The 24th section data from 54 slices obtained by scanning normal to the glass surface. All TR slice images are available in the Supporting Information (Figure S7). The scale bars represent 2 μm.

showed non-negligible Lipi-Blue fluorescence signals (Figure 6D, panel iii). However, photobleaching was not negligible in confocal imaging. Therefore, the Lipi-Blue fluorescence intensities from SLB patches were investigated using epi-fluorescence microscopy, as described in the following section. Notably, in those experiments, photobleaching was negligible.

Epi-Fluorescence Imaging of DOPC and DOPC/DPPC/Cholesterol (3:3:2) SLB Patches Incorporating Oligo(methyl Methacrylate)

The SLB patches were formed on glass by adsorption of vesicles incubated with oligo(methyl methacrylate) droplets.[35,44] Because not all vesicles incorporated the oligomer droplets, droplet-containing and droplet-free bilayer patches were present on the glass surface after vesicle adsorption. These droplet-containing and droplet-free SLB patches were investigated using epi-fluorescence microscopy. In the DOPC sample (Figure 7A), the droplet-containing bilayer patches exhibited high Lipi-Blue fluorescence emission. In contrast, droplet-free bilayer patches located apart from the droplet-containing patches had no significant Lipi-Blue fluorescence emission. However, the droplet-free bilayer patches located near droplet-containing bilayer patches showed relatively large Lipi-Blue fluorescence signals. Therefore, the oligomer molecules appeared to migrate from the bilayer-bound droplets into the aqueous solution and eventually dissolved into nearby bilayer patches. Thus, to reduce the effect of this oligomer incorporation pathway on the statistical data, the Lipi-Blue fluorescence intensities of bilayer patches located >50 μm away from droplets bound to bilayers or on the glass surface were examined. The statistics (Figure 7B) showed that droplet-containing bilayers (red) tended to exhibit larger Lipi-Blue fluorescence signals than the droplet-free bilayers (gray).

https://doi.org/10.1021/acs.langmuir.6c02733
Langmuir 2026, 42, 24915−24925

Downloaded from pubs.acs.org/langd5/article-pdf/42/34/24915/6351340/acs.langmuir.6c02733.pdf by NATL INST FOR MATLS SCIENCE (NIMS), Chiho Kataoka-Hamai on 02 September 2026

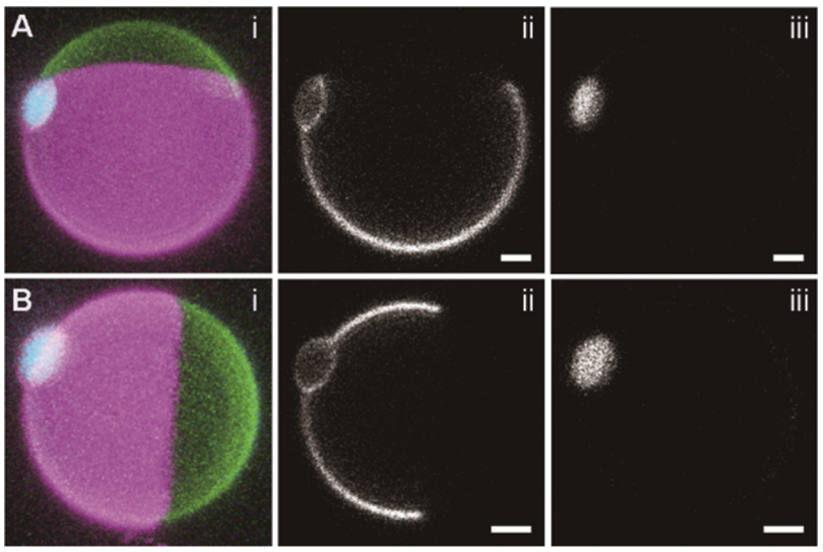


Figure 5. Confocal fluorescence images of DOPC/DPPC/cholesterol (3:3:2) vesicles incorporating an oligo(styrene) droplet. The color images (panel i) are the overlay data for TR-DHPE (magenta), Lipi-Blue (light blue), and NBD-DPPE (green) fluorescence emissions. (A) Fluorescence images of a GUV (diameter: 15.8 μm). (i) The three-dimensional image constructed from 38 slices. (ii, iii) The 13th-slice TR (panel ii) and Lipi-Blue (panel iii) fluorescence images. (B) Fluorescence images of a GUV (diameter: 10.7 μm). (i) The three-dimensional image constructed from 38 slices. (ii, iii) The 17th-slice TR (panel ii) and Lipi-Blue (panel iii) fluorescence images. The scale bars are 2 μm.

These data demonstrate that oligomer migration from the in-bilayer droplets to the matrix bilayer was predominant compared with oligomer absorption from the aqueous solution. The result is consistent with the confocal data (Figure 6B) in which droplet-containing bilayers apparently had higher Lipi-Blue fluorescence intensities than droplet-free bilayers.

In addition, DOPC/DPPC/cholesterol (3:3:2) bilayer patches were investigated (Figure 8). For this lipid composition, droplets bound to the SLB patches did not affect the Lipi-Blue fluorescence intensities of neighboring bilayer patches. SLB patches formed from GUVs before plastic oligomer incorporation showed no significant signals in the Lipi-Blue fluorescence detection channel (Figure S8). In the droplet-containing bilayer patches (Figure 8A), the L_d and L_o phases had considerable Lipi-Blue fluorescence intensities. Therefore, the Lipi-Blue fluorescence intensities of droplet-containing bilayer patches (Figure 8B, red and blue) were compared with those of droplet-free bilayer patches (Figure 8B, gray and black). These data revealed that the droplet-containing bilayers exhibited intense Lipi-Blue fluorescence, whereas the droplet-free bilayers did not. Therefore, the majority of oligomer molecules in the bilayers were likely supplied from the bilayer-binding droplets, rather than from the aqueous solution. Additionally, in the droplet-containing bilayer patches (Figure 8C), the Lipi-Blue fluorescence intensity from the L_d phase (I_d) generally exceeded that from the L_o phase (I_o) (I_d/I_o = 1.23 ($\pm$0.04), N = 30). This finding suggests that the L_d phase contained more oligomers than the L_o phase.

DISCUSSION

The oligo(styrene), oligo(butadiene), and oligo(*tert*-butyl acrylate) droplets were likely surrounded homogeneously by the monolayer leaflets (Figure 9A,B). However, the oligo(methyl methacrylate) droplets were not homogeneously embedded between the monolayer leaflets. This difference might have arisen because oligo(methyl methacrylate) is the most hydrophilic of all investigated oligomers. Notably, triolein and cholesteryl arachidonate droplets were previously shown to be homogeneously embedded within bilayers.[32] These neutral lipids are immiscible with water, but are amphiphilic and form monolayers with phospholipids.[32] The authors' previous and current results therefore show that the nonpolar, hydrophobic molecules (oligo(styrene) and oligo(butadiene)) and the amphiphilic molecules with very low aqueous solubility (oligo(*tert*-butyl acrylate), triolein, and cholesteryl arachidonate) are incorporated in bilayers as droplets surrounded uniformly by monolayer leaflets. In contrast, the non-amphiphilic molecule with relatively high aqueous solubility (oligo(methyl methacrylate)) forms complex aggregates with lipids in bilayers. Therefore, in the present study, the membrane structures obtained after droplet incorporation were likely determined by the hydrophobic/hydrophilic balance of the oil molecule. At low concentrations, highly hydrophobic molecules, such as oligo(styrene) and oligo(butadiene), partition within the hydrophobic region of the bilayer. Above their critical concentration, they aggregate to form a droplet, which is surrounded by the monolayer leaflets. Similarly, amphiphilic molecules (oligo(*tert*-butyl acrylate), triolein, and cholesteryl arachidonate) form droplets homogeneously enclosed by the monolayer leaflets above their critical concentration. At lower concentrations, however, these amphiphilic molecules can align within the bilayer such that their hydrophilic regions orient toward the aqueous phase, whereas their hydrophobic regions are located in the lipid acyl-chain region. In contrast, less hydrophobic molecules, such as oligo(methyl methacrylate), can interact strongly with lipid headgroups, generating complex membrane structures.

The oligo(styrene) and oligo(butadiene) droplets in the DOPC/DPPC (1:1) bilayers were always pinned to domain boundaries (Figure 9A). This pinning is considered to occur in order to decrease the line tension generated along domain boundaries.[45] The thickness of the DPPC bilayer in the S_o phase is larger by ~1.2 nm than that of the DOPC bilayer in the L_d phase.[46] This thickness mismatch results in line tension along the S_o/L_d domain boundaries in the DOPC/DPPC

https://doi.org/10.1021/acs.langmuir.6c02733
Langmuir 2026, 42, 24915−24925

Downloaded from pubs.acs.org/langd5/article-pdf/42/34/24915/6351340/acs.langmuir.6c02733.pdf by NATL INST FOR MATLS SCIENCE (NIMS), Chiho Kataoka-Hamai on 02 September 2026

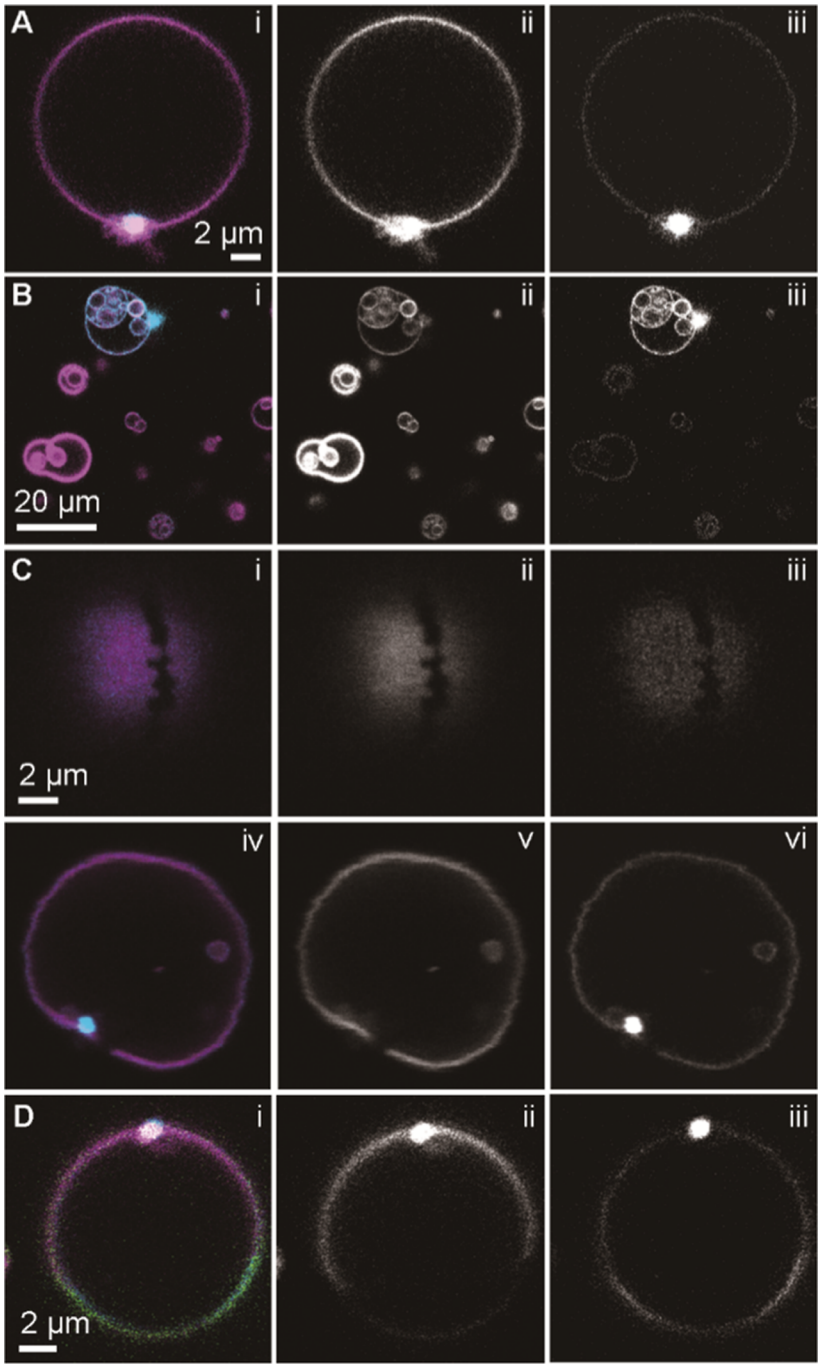


Figure 6. Confocal fluorescence images of (A,B) DOPC/DOPE (9:1), (C) DOPC/DPPC (1:1), and (D) DOPC/DPPC/cholesterol (3:3:2) vesicles exposed to oligo(methyl methacrylate) droplets. The color data (panels i and iv) are the merged images of TR-DHPE (magenta), Lipi-Blue (light blue), and NBD-DPPE (green) fluorescence intensities. The grayscale images are the TR (panels ii and v) and Lipi-Blue (panels iii and vi) channel images. (C) The image slices of the same vesicle obtained near the glass surface (panels i, ii, and iii) and 3.6 μm away from this optical section (panels iv, v, and vi).

mixture.[45] When an oligomer droplet in an L_d-phase bilayer region comes into contact with the boundary against an S_o domain, oligomer molecules penetrate the L_d-phase hydrophobic region near the boundary, increasing the thickness of the L_d-phase bilayer. Consequently, the bilayer thickness mismatch decreases, thereby reducing line tension.

The DOPC/DPPC (1:1) bilayers retained phase separation after incorporating oligo(styrene), oligo(butadiene), and oligo(methyl methacrylate) (Figure 9A,C). However, incorporating oligo(*tert*-butyl acrylate) into the DOPC/DPPC bilayers led to the loss of domain structures (Figure 9B). The results indicate that the DPPC bilayer interacted most strongly with oligo(*tert*-butyl acrylate) among all investigated oligomers. It was expected that oligo(*tert*-butyl acrylate) would be able to disrupt the tightly packed DPPC bilayer structures as a result of its amphiphilic character.

None of the oligomers affected the domain structure in the DOPC/DPPC/cholesterol (3:3:2) bilayer. The oligo(styrene), oligo(butadiene), and oligo(*tert*-butyl acrylate) droplets (Figure 9A,B) were always incorporated into the L_d phase,

https://doi.org/10.1021/acs.langmuir.6c02733
Langmuir 2026, 42, 24915−24925

Downloaded from pubs.acs.org/langd5/article-pdf/42/34/24915/6351340/acs.langmuir.6c02733.pdf by NATL INST FOR MATLS SCIENCE (NIMS), Chiho Kataoka-Hamai on 02 September 2026

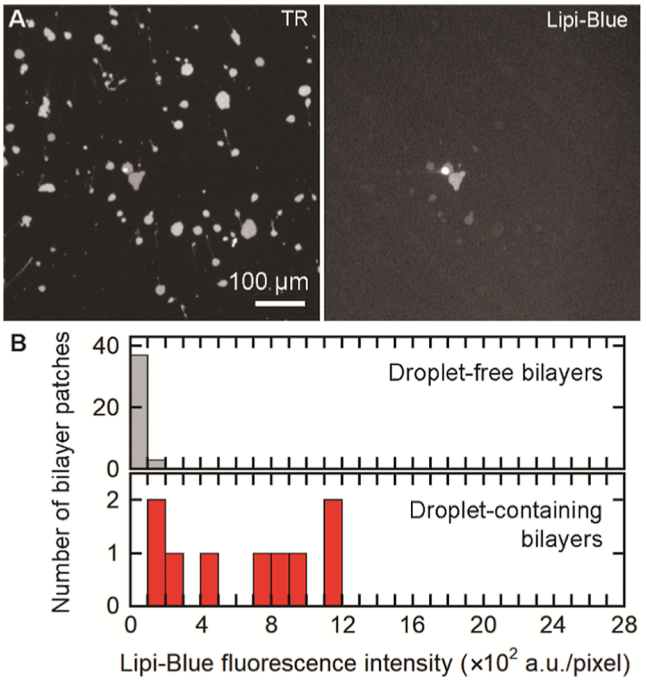


Figure 7. Epi-fluorescence imaging data for SLB patches formed by adsorption of DOPC vesicles incubated with oligo(methyl methacrylate) droplets. (A) TR (left) and Lipi-Blue (right) fluorescence images at 10× magnification. (B) Distributions of the Lipi-Blue fluorescence intensities from SLB patches with (red) or without (gray) droplets measured at 40× magnification. The analyzed droplet-free bilayer patches were located >50 μm away from any bilayer-bound or glass-bound droplets.

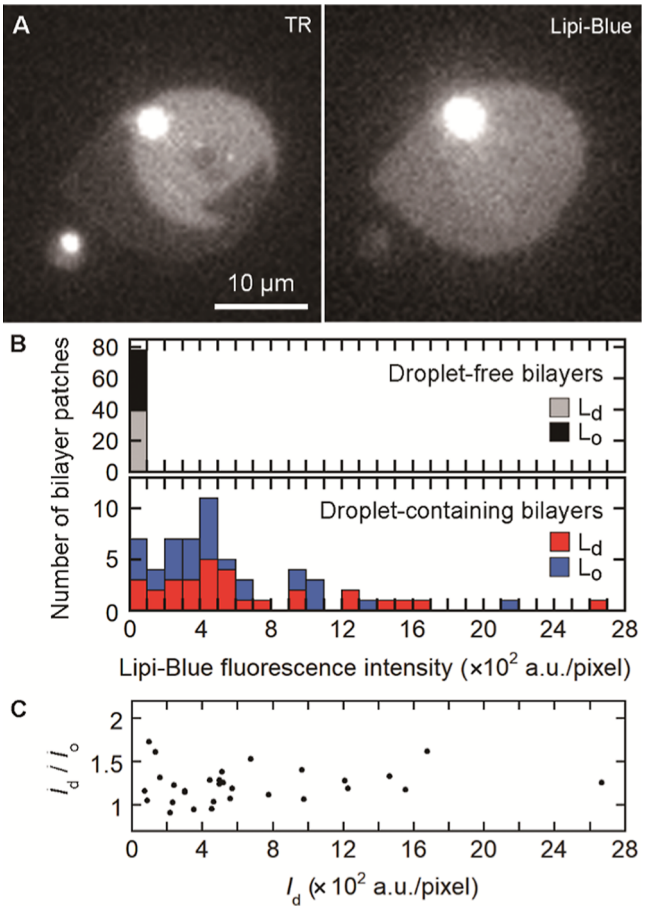


Figure 8. Epi-fluorescence imaging data of SLB patches formed after adsorption of DOPC/DPPC/cholesterol (3:3:2) vesicles exposed to oligo(methyl methacrylate) droplets. (A) TR (left) and Lipi-Blue (right) fluorescence images at 40× magnification. (B) Distributions of the Lipi-Blue fluorescence intensities for the droplet-free (gray, black) and droplet-containing (red, blue) SLB patches obtained at 40× magnification. Data for the L_d-phase domains are represented in gray and red. Data for the L_o-phase domains are represented in black and blue. (C) The ratios between the Lipi-Blue fluorescence intensity of the L_d-phase domain (I_d) and that of the L_o-phase domain (I_o) were determined for the droplet-containing SLB patches in B (red and blue).

with approximately half anchored to domain boundaries. The remaining droplets were located apart from any domain boundaries observed in the fluorescence images. This separation probably occurred because the line tension along the L_d/L_o domain boundary in the DOPC/DPPC/cholesterol (3:3:2) bilayer was smaller than that along the L_d/S_o domain boundary in the DOPC/DPPC (1:1) bilayer. This explanation is supported by a previous study using X-ray diffraction,[47] which showed that the difference in the phosphate-to-phosphate distance across the bilayer between the L_d and L_o domains in DOPC/DPPC/cholesterol (3:3:2) was smaller than that between the L_d and S_o domains in DOPC/DPPC (1:1).

Based on the Lipi-Blue fluorescence intensities from the bilayers, oligo(methyl methacrylate) appeared to have high solubility in the fluid bilayer phases. The significant Lipi-Blue fluorescence emission from the bilayers allowed for identification of the preferred bilayer phase for oligo(methyl methacrylate) penetration. The data suggest that in the DOPC/DPPC (1:1) bilayer (Figure 9C, left), oligo(methyl methacrylate) molecules were predominantly soluble in the L_d phase. However, they were slightly more soluble in the L_d phase than in the L_o phase in the DOPC/DPPC/cholesterol (3:3:2) bilayer (Figure 9C, right). Collectively, in the phase-separated bilayers, oligo(methyl methacrylate) molecules diffused more readily into the loosely packed and more-fluid phase than the tightly packed and less-fluid phase. These oligomers may aggregate to form nanometer-sized particles within the bilayers. However, whether such aggregation occurred remains unclear.

Finally, two pathways allowing the incorporation of oligo(methyl methacrylate) in the DOPC and DOPC/DOPE (9:1) bilayers were observed (Figures 6B and 7). In one pathway, the transfer of oligomer molecules from a bilayer-bound droplet to the matrix bilayer occurred via diffusion across the membrane structures. In the other pathway, the free oligomer molecules were absorbed from the aqueous solution. The former mechanism appears to be predominant compared with the latter.

CONCLUSIONS

Oligo(styrene), oligo(butadiene), and oligo(*tert*-butyl acrylate) droplets were homogeneously incorporated within the bilayers. However, the oligo(methyl methacrylate) droplets were associated with the bilayers through complex membrane structures. In addition, the domain structures in the DOPC/DPPC (1:1) and DOPC/DPPC/cholesterol (3:3:2) bilayers were unchanged after incorporating each oligomer, except in the case of DOPC/DPPC (1:1) vesicles with oligo(*tert*-butyl

https://doi.org/10.1021/acs.langmuir.6c02733
Langmuir 2026, 42, 24915−24925

Downloaded from pubs.acs.org/langd5/article-pdf/42/34/24915/6635134O/acs.langmuir.6c02733.pdf by NATL INST FOR MATLS SCIENCE (NIMS), Chiho Kataoka-Hamai on 02 September 2026

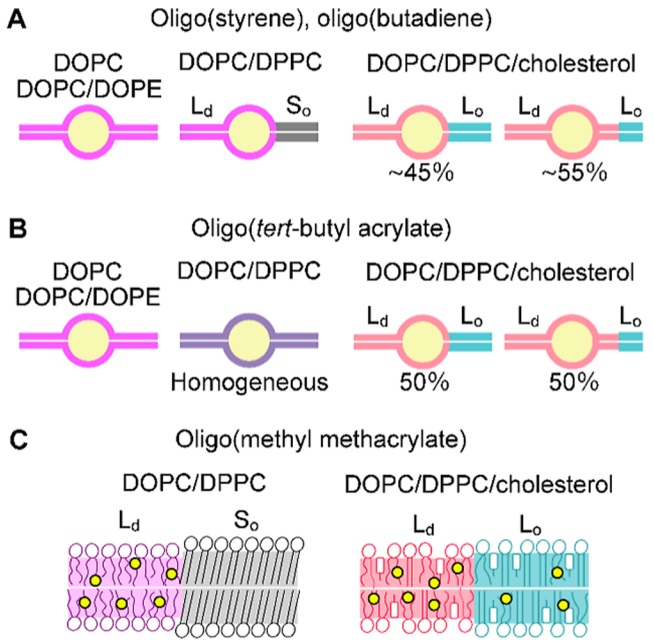


Figure 9. Schematics illustrating plastic oligomer incorporation into the DOPC, DOPC/DOPE (9:1), DOPC/DPPC (1:1), and DOPC/DPPC/cholesterol (3:3:2) bilayers. (A) Distributions of oligo(styrene) and oligo(butadiene) droplets (yellow). (B) Distributions of oligo(*tert*-butyl acrylate) droplets (yellow). (C) Distributions of oligo(methyl methacrylate) molecules (yellow).

acrylate) droplets. In the latter case, the fluorescence images showed no domain structures. In the L_d/S_o phase-separated bilayer, the oligo(styrene) and oligo(butadiene) droplets were always partitioned in the L_d phase and also pinned at the domain boundaries. In contrast, oligo(styrene), oligo(butadiene), and oligo(*tert*-butyl acrylate) droplets in the L_d/L_o phase-separated bilayer were located exclusively in the L_d phase, with approximately half anchored to domain boundaries. Droplet pinning at L_d/S_o and L_d/L_o domain boundaries likely occurred to decrease line tension along domain boundaries. In addition, in the phase-separated bilayers, the oligo(methyl methacrylate) molecules were more soluble in the loosely packed L_d phase than in the tightly packed S_o or L_o phase. Finally, there were two pathways for incorporating oligo(methyl methacrylate) molecules into the DOPC and DOPC/DOPE (9:1) bilayers. One pathway was oligomer diffusion from a bilayer-bound droplet to the same bilayer. The other pathway was oligomer uptake from the aqueous solution. The second pathway was possible because the oligo(methyl methacrylate) was slightly soluble in water. These various oligomer behaviors are expected to result from differences in the degree of hydrophobicity, amphiphilicity, and aqueous solubility.

■ ASSOCIATED CONTENT

Supporting Information

The Supporting Information is available free of charge at https://pubs.acs.org/doi/10.1021/acs.langmuir.6c02733.

^{1}H NMR spectra of oligo(methyl methacrylate), confocal fluorescence images of GUVs before plastic oligomer incorporation, confocal fluorescence images of DOPC/DOPE (9:1) GUVs incorporating oligo(styrene), oligo(butadiene), and oligo(*tert*-butyl acrylate) droplets, all the optical sections recorded for the GUV in Figure 4C, and epi-fluorescence images of a DOPC/DPPC/cholesterol (3:3:2) SLB patch in the absence of plastic oligomers (PDF)

■ AUTHOR INFORMATION

Corresponding Author

Chiho Kataoka-Hamai − *Research Center for Macromolecules and Biomaterials, National Institute for Materials Science, Ibaraki 305-0044, Japan;* orcid.org/0000-0002-4068-0405; Email: kataoka.chiho@nims.go.jp

Authors

Waka Nakanishi − *Research Center for Macromolecules and Biomaterials, National Institute for Materials Science, Ibaraki 305-0047, Japan;* orcid.org/0000-0001-6801-1839

Shinya Hattori − *Advanced Engineering and Services Division, National Institute for Materials Science, Ibaraki 305-0047, Japan*

Complete contact information is available at: https://pubs.acs.org/10.1021/acs.langmuir.6c02733

Notes

The authors declare no competing financial interest.

■ ACKNOWLEDGMENTS

This work was supported by the Advanced Research Infrastructure for Materials and Nanotechnology in Japan (ARIM) program of the Ministry of Education, Culture, Sports, Science and Technology (MEXT) (Proposal Number JPMXP1225NM5501).

■ REFERENCES

(1) Geyer, R.; Jambeck, J. R.; Law, K. L. Production, Use, and Fate of All Plastics Ever Made. *Sci. Adv.* **2017**, *3*, No. e1700782.

(2) Jambeck, J. R.; Geyer, R.; Wilcox, C.; Siegler, T. R.; Perryman, M.; Andrady, A.; Narayan, R.; Law, K. L. Plastic Waste Inputs from Land into the Ocean. *Science* **2015**, *347*, 768−771.

(3) Thompson, R. C.; Courtene-Jones, W.; Boucher, J.; Pahl, S.; Raubenheimer, K.; Koelmans, A. A. Twenty Years of Microplastic Pollution Research What Have We Learned? *Science* **2024**, *386*, No. eadl2746.

(4) MacLeod, M.; Arp, H. P. H.; Tekman, M. B.; Jahnke, A. The Global Threat from Plastic Pollution. *Science* **2021**, *373*, 61−65.

(5) Hartmann, N. B.; Hüffer, T.; Thompson, R. C.; Hassellöv, M.; Verschoor, A.; Daugaard, A. E.; Rist, S.; Karlsson, T.; Brennholt, N.; Cole, M.; et al. Are We Speaking the Same Language? Recommendations for a Definition and Categorization Framework for Plastic Debris. *Environ. Sci. Technol.* **2019**, *53*, 1039−1047.

(6) Hirai, H.; Takada, H.; Ogata, Y.; Yamashita, R.; Mizukawa, K.; Saha, M.; Kwan, C.; Moore, C.; Gray, H.; Laursen, D.; et al. Organic Micropollutants in Marine Plastics Debris from the Open Ocean and Remote and Urban Beaches. *Mar. Pollut. Bull.* **2011**, *62*, 1683−1692.

(7) Mato, Y.; Isobe, T.; Takada, H.; Kanehiro, H.; Ohtake, C.; Kaminuma, T. Plastic Resin Pellets as a Transport Medium for Toxic Chemicals in the Marine Environment. *Environ. Sci. Technol.* **2001**, *35*, 318−324.

(8) Shi, C.; Wang, M.; Wang, Z.; Qu, G.; Jiang, W.; Pan, X.; Fang, M. Oligomers from the Synthetic Polymers: Another Potential Iceberg of New Pollutants. *Environ. Health* **2023**, *1*, 228−235.

(9) Shi, C. Z.; Guo, A.; Pang, S. C.; Yang, J.; Liu, M.; Zhao, F.; Wang, M. J.; Dou, X. H.; Sui, Q.; Xu, C. R.; et al. Precise Characterization of the Presence and Fate of Plastic Oligomers in Water. *Nat. Water* **2025**, *3*, 461−472.

Downloaded from pubs.acs.org/langd5/article-pdf/42/34/24915/6351340/acs.langmuir.6c02733.pdf by NATL INST FOR MATLS SCIENCE (NIMS), Chiho Kataoka-Hamai on 02 September 2026

(10) Wang, M. J.; Li, Q. Q.; Shi, C. Z.; Lv, J.; Xu, Y. D.; Yang, J. J.; Chua, S. L.; Jia, L. R.; Chen, H. W.; Liu, Q.; et al. Oligomer Nanoparticle Release from Polylactic Acid Plastics Catalysed by Gut Enzymes Triggers Acute Inflammation. *Nat. Nanotechnol.* **2023**, *18*, 403−411.
(11) Yoshinaga, N.; Tateishi, A.; Kobayashi, Y.; Kubo, T.; Miyakawa, H.; Satoh, K.; Numata, K. Effect of Oligomers Derived from Biodegradable Polyesters on Eco-and Neurotoxicity. *Biomacromolecules* **2023**, *24*, 2721−2729.
(12) Bochicchio, D.; Panizon, E.; Monticelli, L.; Rossi, G. Interaction of Hydrophobic Polymers with Model Lipid Bilayers. *Sci. Rep.* **2017**, *7*, 6357.
(13) Lazarski, G.; Rajtar, N.; Romek, M.; Jamróz, D.; Rawski, M.; Kepczynski, M. Interaction of Polystyrene Nanoplastic with Lipid Membranes. *J. Phys. Chem. B* **2025**, *129*, 4110−4122.
(14) Piskulich, Z. A.; Rosenzweig, Z.; Cui, Q. Polystyrene-Induced Dehydration of Lipid Membranes: Insights from Atomistic Simulations. *J. Phys. Chem. B* **2025**, *129*, 8724−8731.
(15) Rossi, G.; Barnoud, J.; Monticelli, L. Polystyrene Nanoparticles Perturb Lipid Membranes. *J. Phys. Chem. Lett.* **2014**, *5*, 241−246.
(16) Duraes, A. D. S.; Jiao, E. L.; Zhang, W. L. Effects of Nanoplastics on Lipid Membranes and Vice Versa: Insights from All-Atom Molecular Dynamics Simulations. *J. Phys. Chem. B* **2025**, *129*, 3385−3395.
(17) Holloczki, O.; Gehrke, S. Can Nanoplastics Alter Cell Membranes? *ChemPhysChem* **2020**, *21*, 9−12.
(18) Munafò, I.; Costa, D.; Milano, G.; Munaò, G. Absorption of Polypropylene in Dipalmitoylphosphatidylcholine Membranes: The Role of Molecular Weight and Initial Configuration of Polymer Chains. *J. Phys. Chem. B* **2024**, *128*, 9905−9916.
(19) Järvenpää, J.; Perkkiö, M.; Laitinen, R.; Lahtela-Kakkonen, M. PE and PET Oligomers' Interplay with Membrane Bilayers. *Sci. Rep.* **2022**, *12*, 2234.
(20) Fleury, J. B.; Baulin, V. A. Microplastics Destabilize Lipid Membranes by Mechanical Stretching. *Proc. Natl. Acad. Sci. U.S.A.* **2021**, *118*, No. e2104610118.
(21) Chairil, R.; Zachariah, S.; Malmstadt, N. Nanoplastic Shape Effects on Lipid Bilayer Permeabilization. *Environ. Sci. Technol.* **2025**, *59*, 23751−23761.
(22) Morandi, M. I.; Kluzek, M.; Wolff, J.; Schroder, A.; Thalmann, F.; Marques, C. M. Accumulation of Styrene Oligomers Alters Lipid Membrane Phase Order and Miscibility. *Proc. Natl. Acad. Sci. U.S.A.* **2021**, *118*, No. e2016037118.
(23) Yuan, Z. H.; Nag, R.; Cummins, E. Ranking of Potential Hazards from Microplastics Polymers in the Marine Environment. *J. Hazard. Mater.* **2022**, *429*, 128399.
(24) Leslie, H. A.; van Velzen, M. J. M.; Brandsma, S. H.; Vethaak, A. D.; Garcia-Vallejo, J. J.; Lamoree, M. H. Discovery and Quantification of Plastic Particle Pollution in Human Blood. *Environ. Int.* **2022**, *163*, 107199.
(25) Yang, Y. X.; Xie, E. Z. H.; Du, Z. Y.; Peng, Z.; Han, Z. Y.; Li, L. Y.; Zhao, R.; Qin, Y. W.; Xue, M. Q.; Li, F. W.; et al. Detection of Various Microplastics in Patients Undergoing Cardiac Surgery. *Environ. Sci. Technol.* **2023**, *57*, 10911−10918.
(26) Kwon, B. G.; Koizumi, K.; Chung, S. Y.; Kodera, Y.; Kim, J. O.; Saido, K. Global Styrene Oligomers Monitoring as New Chemical Contamination from Polystyrene Plastic Marine Pollution. *J. Hazard. Mater.* **2015**, *300*, 359−367.
(27) Kwon, B. G.; Yan, B. Aquatic Toxicity and Fate of Styrene Oligomers in the Environment. *Ecotoxicol. Environ. Saf.* **2023**, *265*, 115462.
(28) Ziajahromi, S.; Lu, H. C.; Drapper, D.; Hornbuckle, A.; Leusch, F. D. L. Microplastics and Tire Wear Particles in Urban Stormwater: Abundance, Characteristics, and Potential Mitigation Strategies. *Environ. Sci. Technol.* **2023**, *57*, 12829−12837.
(29) Dibke, C.; Fischer, M.; Scholz-Böttcher, B. M. Microplastic Mass Concentrations and Distribution in German Bight Waters by Pyrolysis−Gas Chromatography-Mass Spectrometry/Thermochemolysis Reveal Potential Impact of Marine Coatings: Do Ships Leave Skid Marks? *Environ. Sci. Technol.* **2021**, *55*, 2285−2295.
(30) Chorlay, A.; Thiam, A. R. An Asymmetry in Monolayer Tension Regulates Lipid Droplet Budding Direction. *Biophys. J.* **2018**, *114*, 631−640.
(31) Kataoka-Hamai, C. Triacylglycerol-Droplet-Induced Bilayer Spontaneous Curvature in Giant Unilamellar Vesicles. *Biophys. J.* **2024**, *123*, 1857−1868.
(32) Kataoka-Hamai, C.; Song, J. W.; Kawakami, K. Incorporation of Triacylglycerol and Cholesteryl Ester Droplets in Phase-Separated Giant Unilamellar Vesicles. *Langmuir* **2025**, *41*, 6113−6123.
(33) Chen, P. S.; Toribara, T. Y.; Warner, H. Microdetermination of Phosphorus. *Anal. Chem.* **1956**, *28*, 1756−1758.
(34) Tatenaka, Y.; Kato, H.; Ishiyama, M.; Sasamoto, K.; Shiga, M.; Nishitoh, H.; Ueno, Y. Monitoring Lipid Droplet Dynamics in Living Cells by Using Fluorescent Probes. *Biochemistry* **2019**, *58*, 499−503.
(35) Kataoka-Hamai, C.; Kawakami, K. Domain Sorting in Giant Unilamellar Vesicles Adsorbed on Glass. *Langmuir* **2021**, *37*, 1082−1088.
(36) Witkowska, A.; Jablonski, L.; Jahn, R. A Convenient Protocol for Generating Giant Unilamellar Vesicles Containing SNARE Proteins Using Electroformation. *Sci. Rep.* **2018**, *8*, 9422.
(37) Mabrey, S.; Sturtevant, J. M. Investigation of Phase-Transitions of Lipids and Lipid Mixtures by High Sensitivity Differential Scanning Calorimetry. *Proc. Natl. Acad. Sci. U.S.A.* **1976**, *73*, 3862−3866.
(38) Veatch, S. L.; Keller, S. L. Separation of Liquid Phases in Giant Vesicles of Ternary Mixtures of Phospholipids and Cholesterol. *Biophys. J.* **2003**, *85*, 3074−3083.
(39) Schindelin, J.; Arganda-Carreras, I.; Frise, E.; Kaynig, V.; Longair, M.; Pietzsch, T.; Preibisch, S.; Rueden, C.; Saalfeld, S.; Schmid, B.; et al. Fiji: An Open-Source Platform for Biological-Image Analysis. *Nat. Methods* **2012**, *9*, 676−682.
(40) Anzai, T.; Kawauchi, M.; Kawauchi, T.; Kumaki, J. Crystallization Behavior of Single Isotactic Poly(methyl methacrylate) Chains Visualized by Atomic Force Microscopy. *J. Phys. Chem. B* **2015**, *119*, 338−347.
(41) Kumaki, J.; Kawauchi, T.; Yashima, E. Two-Dimensional Folded Chain Crystals of a Synthetic Polymer in a Langmuir-Blodgett Film. *J. Am. Chem. Soc.* **2005**, *127*, 5788−5789.
(42) Li, S.; Hanley, S.; Khan, I.; Varshney, S. K.; Eisenberg, A.; Lennox, R. B. Surface Micelle Formation at the Air/Water Interface from Nonionic Diblock Copolymers. *Langmuir* **1993**, *9*, 2243−2246.
(43) Himeno, H.; Shimokawa, N.; Komura, S.; Andelman, D.; Hamada, T.; Takagi, M. Charge-Induced Phase Separation in Lipid Membranes. *Soft Matter* **2014**, *10*, 7959−7967.
(44) Hamai, C.; Cremer, P. S.; Musser, S. M. Single Giant Vesicle Rupture Events Reveal Multiple Mechanisms of Glass-Supported Bilayer Formation. *Biophys. J.* **2007**, *92*, 1988−1999.
(45) Kuzmin, P. I.; Akimov, S. A.; Chizmadzhev, Y. A.; Zimmerberg, J.; Cohen, F. S. Line Tension and Interaction Energies of Membrane Rafts Calculated from Lipid Splay and Tilt. *Biophys. J.* **2005**, *88*, 1120−1133.
(46) Nagle, J. F.; Tristram-Nagle, S. Structure of Lipid Bilayers. *Biochim. Biophys. Acta, Biomembr.* **2000**, *1469*, 159−195.
(47) Ma, Y. C.; Ghosh, S. K.; DiLena, D. A.; Bera, S.; Lurio, L. B.; Parikh, A. N.; Sinha, S. K. Cholesterol Partition and Condensing Effect in Phase-Separated Ternary Mixture Lipid Multilayers. *Biophys. J.* **2016**, *110*, 1355−1366.

Downloaded from pubs.acs.org/langd5/article-pdf/42/34/24915/6635134O/acs.langmuir.6c02733.pdf by NATL INST FOR MATLS SCIENCE (NIMS), Chiho Kataoka-Hamai on 02 September 2026

https://doi.org/10.1021/acs.langmuir.6c02733
Langmuir 2026, 42, 24915−24925